Resonant x-ray scattering studies of the magnetic structure near the surface of an antiferromagnet

G. M. Watson
Department of Physics, University of Maryland Baltimore County, Baltimore, Maryland 21250

Doon Gibbs
Department of Physics, Brookhaven National Laboratory, Upton, New York 11973-5000

G. H. Lander
European Commission, Joint Research Center, Institute for Transuranium Elements, Postfach 2340, D-76125 Karlsruhe, Germany

B. D. Gaulin
Department of Physics and Astronomy, McMaster University, Hamilton, Ontario, Canada L8S 4M1

L. E. Berman
National Synchrotron Light Source, Brookhaven National Laboratory, Upton, New York 11973-5000

Hj. Matzke
European Commission, Joint Research Center, Institute for Transuranium Elements, Postfach 2340, D-76125 Karlsruhe, Germany

W. Ellis
Los Alamos National Laboratory, Los Alamos, New Mexico 87545
(Received 18 October 1999)

Resonant x-ray magnetic scattering is used to study magnetic order near the (001) surface of the antiferromagnetic oxide UO_2 for temperatures between 10 and 35 K. It is found that for temperatures below the bulk Néel temperature a magnetically disordered region exists at the surface, and is separated from the magnetically ordered bulk by a diffuse magnetic interface. The width of the magnetic interface is temperature dependent, and appears to diverge as the sample temperature approaches the bulk Néel temperature. In contrast to the bulk, which exhibits a discontinuous magnetic ordering transition, the surface layers order continuously. These results are shown to be qualitatively consistent with the theory of surface induced disorder.

I. INTRODUCTION

The magnetic properties of surfaces and interfaces have recently become a topic of great interest, in part due to the technological importance of spin-engineered thin-film devices.[1] Coincident with this attention has been the development of techniques for the study of magnetism in thin films and at surfaces. Several of these techniques utilize photons in the soft and hard x-ray wavelength regimes, and rely on resonant processes, which occur when the incident photon energy is tuned near an absorption edge. The magnetic sensitivity is due to a virtual electronic transition from a spin-orbit split core level into spin-polarized final states. Whereas a number of these techniques have the sensitivity required to measure the magnetization of films as thin as a single monolayer,[2] and others are directly sensitive to surface magnetism,[3] few are able to determine how the magnetization changes as a function of distance from the surface or interface.[4] In this regard, resonant x-ray and neutron magnetic reflectivity techniques appear unique.[5]

In this paper, we illustrate how resonant x-ray magnetic reflectivity may be used to obtain sublattice magnetization profiles at the surface of a bulk antiferromagnet, in particular, at the (001) surface of UO_2. We then describe experiments in which the magnetic reflectivity is used to study antiferromagnetic disordering near the surface as a function of temperature. Our motivations for the experiments were, first, to determine whether antiferromagnetic truncation rods could be observed by x-ray scattering and, second, to study the effect of the surface on a bulk magnetic order-disorder phase transformation.

Earlier studies utilizing soft x-ray resonance techniques have also characterized the magnetic specular reflectivity, mainly near the L absorption edges of $3d$ transition elements. For example, Kao *et al.*,[6] observed the change in reflectivity vs momentum transfer from an iron film when the magnetization was flipped by 180°, and related it to the interfacial magnetic structure. Since then, a number of related experiments have been performed at the L edges of other $3d$ transition metals.[7–9] As a result of the long wavelength of the photons at these edges, the measurements have been limited to magnetic structures with unit cells larger than $\approx$10 Å.

In order to benefit from the large resonant enhancement of the magnetic scattering at the M absorption edges of uranium compounds,[10] we decided to look for the magnetic truncations rods of UO_2. In addition, for antiferromagnetic samples, some of the magnetic rods exist separately from the chemical truncation rods. In contrast, the magnetic and

chemical periods of ferromagnets are identical so that the bulk charge and magnetic truncation rods overlap in reciprocal space. To observe ferromagnetic rods therefore it is necessary to perform difference experiments in which Bragg intensities are measured for two directions of an applied magnetic field, or for right and left circularly polarized incident beams. In an elegant set of experiments on the ferromagnetic alloy CoPt, Ferrer *et al.* recently related the induced magnetism of Pt atoms at the surface to the surface stoichiometery by working at the Pt L_{III} edge.[11] By measuring the flipping ratio over a large portion of the truncation rod they were able to show that the magnetization of the Pt atoms at the surface is reduced from that in the bulk.

There has been considerable interest in magnetic phase transitions at surfaces during the last 30 years. Perhaps the best studied examples are the (001) and (110) surfaces of Ni and the (001) surface of Gd, which have all been characterized using spin-polarized low-energy electron diffraction. The exponent β_s, which describes the temperature dependence of the surface order parameter, has been determined for Ni(001).[12] It was found that its value at the surface ($\beta_s = 0.825$) differs considerably from that of the bulk ($\beta_b = 0.33$). The Gd (001) surface exhibits the remarkable property of surface freezing,[13] that is, it is magnetically ordered at temperatures *above* the bulk Curie temperature. Unfortunately, in neither case was it possible to determine how the near surface magnetic order couples to the underlying bulk magnetic order.

For UO_2(001) surfaces at low temperatures, we show that a magnetically disordered region exists at the surface. This disordered region is separated from the ordered bulk by a magnetic interface. At the lowest temperatures studied the interface is diffuse and has a width of approximately 6 Å. As the temperature increases towards the bulk Néel temperature, the thickness of the disordered surface layer remains constant while the width of the diffuse magnetic interface appears to diverge. In addition, the temperature dependence of the magnetic intensities at the surface vary continuously near the transition, in contrast to the bulk, which is discontinuous. These intriguing results are qualitatively consistent with the theory of surface induced disorder put forward by Lipowsky and co-workers,[14,15] and summarized by Schweika, *et al.*[16] Surface induced disorder has previously been observed in x-ray scattering studies of alloy ordering at the Cu_3Au surface.[17,18] The present paper describes our earlier results obtained for UO_2(001) in more detail,[19] together with more recent experiments which help clarify the nature of the disordering near the surface.

II. EXPERIMENTAL PROCEDURES

A. Experiment

The experiments described here were carried out using Beamlines X22C and X25 at the National Synchrotron Light Source (NSLS). At beamline X22C, approximately 6 mrad of radiation from a bending magnet were focused by a Ni-coated, bent, cylindrical mirror into a spot approximately 1 mm in diameter at the sample. Monochromatic x rays set at the energy of the U M_{IV} edge (3.728 keV) were selected by a double crystal Ge(111) monochromator. At these energies, the incident flux on the sample is estimated to be $\sim 1 \times 10^{10}$ photons per second. At the insertion device beamline X25, approximately 2×10^{11} photons per second are incident on the sample, and focused into a spot of 0.5 mm^2 by a platinum coated silicon mirror. A nondispersive, two-crystal Si(111) monochromator with adaptive optics was employed to tune the photon energy to the uranium M_{IV} edge. The experiments were performed with a standard four-circle vertical-scattering diffractometer at X25 and with a six-circle diffractometer at X22C.

Two different samples were characterized. Both were cut and polished to produce a surface aligned to within $\pm 0.25°$ of the (001) direction. The first sample (sample 1), used in the majority of the work, was provided by Los Alamos National Laboratory. The second sample (sample 2) came from the European Institute for Transuranium Elements. Prior to these measurements, both samples were annealed at 1400 °C in a reducing atmosphere, consisting of 3.5% hydrogen and 96.5% Ar. The anneal served to reduce any near surface damage produced in the polishing process and to guarantee a bulk oxygen stoichiometry of UO_2. All of the magnetic scattering experiments were performed with sample 1 mounted in a Be can backfilled with He exchange gas. Temperature control was achieved by means of a closed-cycle He refrigerator for which the temperature stability was ~ 0.02 K over periods of hours. The bulk mosaic was measured to be 0.05° at the (002) reflection.

The incident x rays were linearly polarized with the electric field in the horizontal plane.[10] Both specular and nonspecular truncation rods were characterized. Specular scattering was carried out in a vertical scattering plane whereas the scattering plane for nonspecular measurements had a small horizontal component. Two types of detectors, a simple linear detector and a standard Bicron detector, were used to determine the intensity of the rods along the surface normal direction. Since charge and magnetic scattering overlap along the specular direction, it was necessary to use a polarization analyzer to isolate the magnetic reflectivity. For linearly σ polarized incident x rays, the polarization of the magnetic scattering in UO_2(001) is rotated by 90°, whereas the charge scattering remains unrotated.[20] A Au(111) crystal was used to analyze the polarization of the scattered beam, and thereby to discriminate against charge scattering.[21] At the U M_{IV} edge, the scattering angle of the Au analyzer is 89.8°.

B. Bulk magnetic structure

UO_2 has the CaF_2 crystal structure [see Fig. 1(a)] with a lattice constant of 5.47 Å at room temperature. The bulk structure consists of U^{4+} ions arranged on an fcc lattice each with eight nearest-neighbor O^{2-} ions. UO_2 is a type-I antiferromagnet with a discontinuous magnetic-ordering transformation at $T_N \sim 30.2$ K.[22–24] The bulk magnetic structure consists of ferromagnetically aligned (001)-type atomic planes, stacked antiferromagnetically along the [001] direction. UO_2 is also triple *q*, which means that all three (001)-type magnetic modulations exist simultaneously within a single domain. The magnetic order associated with one of the three coexisting magnetic modulations is shown in Fig. 1(a).

A representation of the bulk allowed Bragg reflections in the $(001) \times (010)$ plane is shown by the solid circles in Fig.

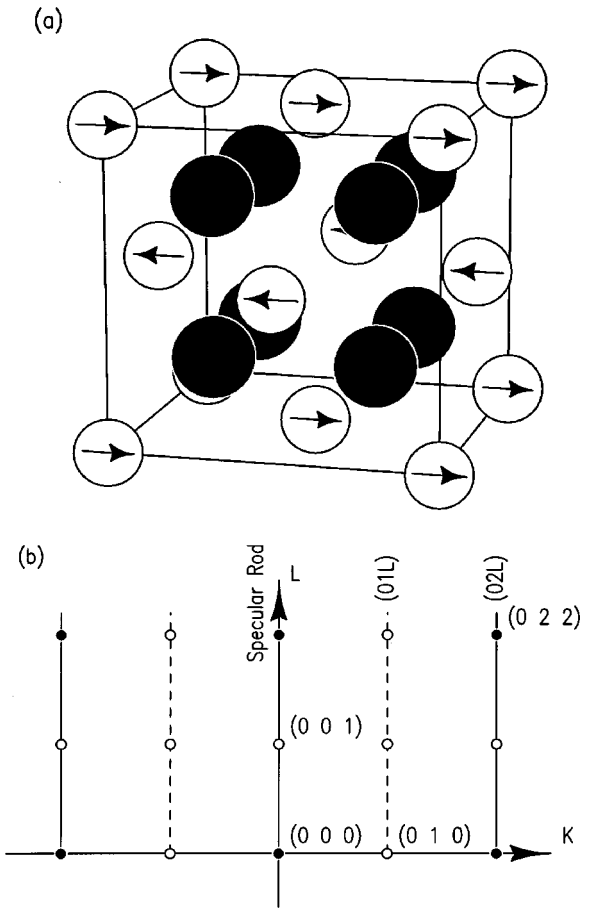

FIG. 1. (a) Crystal and magnetic structure of UO_2. The U atoms (open spheres) occupy an fcc lattice with a room-temperature lattice constant of $a=5.47$ Å. The oxygen atoms (solid spheres) sit on a simple cubic lattice offset from the U lattice by $(\frac{1}{4}, \frac{1}{4}, \frac{1}{4})$. The arrows represent one component of the triple q antiferromagnetic structure. It should be noted that the orientation of the moments within the (001) planes is not known, but they do lie in the plane perpendicular to the propagation direction **q**. (b) Reciprocal space map for the UO_2 (001) surface showing charge (solid circles) and magnetic (open circles) bulk Bragg reflections. Magnetic truncation rods (dashed lines) and truncation rods with both magnetic and charge components (solid lines) are also shown.

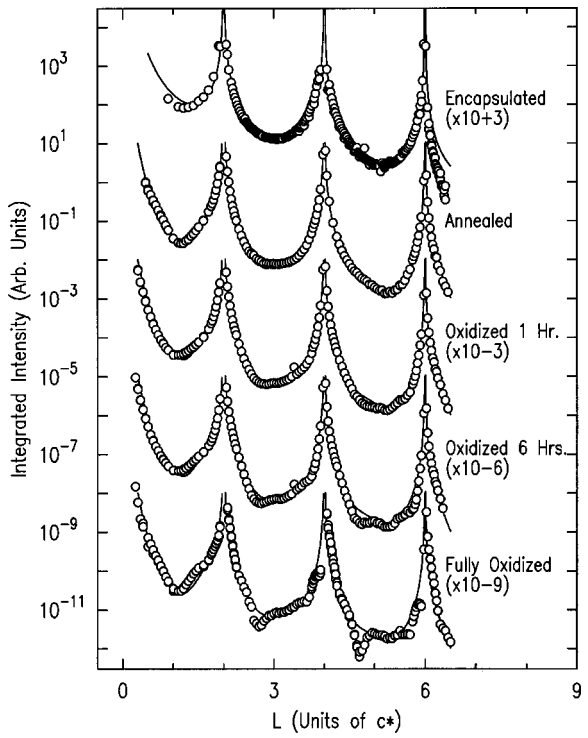

FIG. 2. Specular x-ray reflectivity from UO_2 (001) surfaces after various surface preparations, plotted vs momentum transfer L. Data are shown by the open circles. Solid lines show fits to the encapsulated and annealed data, which correspond to bulk truncation. Curves have been offset for clarity. The singularities at $L=2$, 4, 6 correspond to bulk allowed Bragg reflections. The geometry of the scattering is illustrated in the figure.

1(b). When the sample is cooled to temperature below T_N, additional bulk Bragg reflections appear, arising from the magnetic structure. The allowed magnetic bulk Bragg reflections are displaced from the atomic Bragg reflections by a [001]-type wave vector, and are shown by the open circles in Fig. 1(b). Truncation rods are defined as rods of scattering which lie along the surface normal direction and pass through the bulk Bragg reflections.[25] In Fig. 1(b), the solid lines are rods resulting from the chemical or atomic structure of the surface, which we will call chemical truncation rods. In analogy with the chemical truncation rods, one may also define magnetic truncation rods aligned along the surface normal and passing through the magnetic bulk Bragg reflections.[5] Their existence originates in the truncation of the magnetic structure at the surface. The dashed lines in Fig. 1(b) show the expected pure bulk magnetic truncation rods. Since the solid lines also pass through magnetic bulk Bragg reflections, they will have both a magnetic and a charge contribution for temperatures below T_N. We refer to these rods as being mixed. For UO_2, $a*=b*=c*=2\pi/a=1.14$ Å^{-1} at room temperature.

C. Surface preparation and characterization

Due in part to the importance of the material as a fuel in nuclear reactors, surfaces of UO_2 have been studied for many years.[26–28] Along the [001] direction, the ideally terminated UO_2 structure consists of alternating planes of U^{4+} and O^{2-} ions [see Fig. 1(b)]. It has been shown, however, that clean, stable surfaces with a $c(2\times2)$ reconstruction can be prepared in vacuum.[27] Because the sample is an oxide, and relatively inert, we originally thought that exposure to air would not significantly alter the surface properties. Accordingly, none of our experiments were performed in ultrahigh vacuum. More recently, we have initiated simple tests of these assumptions. As shown in Fig. 2, the x-ray reflectivity[25,29] from the chemical surface is unaltered when the exposure to atmosphere is for a time less than 1 h, but it evolves on a time scale of hours and days. Fits of the magnetic reflectivity (discussed in Sec. III) suggest that an approximately 10-Å-thick region near the surface is altered upon exposure to air for more than two weeks. Allen showed that exposure of polycrystalline surfaces to oxygen[26] produces $UO_{2+\delta}$ with $0\leqslant\delta\leqslant0.25$. We infer from this that the near surface region of the surfaces studied in our experiments may possess an oxygen stoichiometry just greater than 2. For comparison, the specular reflectivity expected from a bulk terminated surface is shown by the solid line in Fig. 2.

To characterize the stability of this surface upon exposure to air, and to eventually learn how to prepare better surfaces, sample 2 was mounted in a vacuum chamber held at 10^{-5} torr. The sample was annealed *in situ* in the H_2/Ar mixture at 200–300 °C. Following the anneal, the x-ray specular reflectivity showed nearly perfect bulk truncation. This data is labeled ''annealed'' in Fig. 2. The sample was then exposed to air for 1 h, after which the vacuum chamber was pumped down and another set of specular reflectivity data taken. This procedure was repeated for a total exposure to air of 6 h. The reflectivity curves for these surfaces are also included in Fig. 2. From the figure it appears that the oxidization of the annealed surface is continuous and that only slight changes in the surface have occurred for exposure times of the order of an hour.

Based on these results, sample 1 was vacuum annealed and sealed in the Be can with less than 5 min exposure to air. The specular reflectivity taken more than three months after the anneal is labeled ''encapsulated'' in Fig. 2. The best fit to this data (solid line) indicates that the surface is atomically flat in domains greater than 1000 Å, which is the x-ray coherence length, and has an outermost *U-U* spacing within 2% of the bulk value. Because the scattering of x rays by uranium is considerably stronger than that of oxygen, we were unable to determine if the surface was terminated by oxygen or uranium.

All of the magnetic scattering data reported in this paper were obtained from the slightly oxidized surface. Preliminary measurements of the encapsulated sample have shown a significant enhancement of the magnetic scattering intensity along the truncation rods relative to the oxidized sample, and will be published separately. The widths of the magnetic truncation rods appear to be the same in both cases, which suggests, but does not prove that the in-plane structures are similar in the two samples. We attribute the reduced intensity along the magnetic truncation rod in the present sample to the x-ray attenuation by the layer of higher oxide.

D. X-ray resonant magnetic reflectivity

In this section we describe the resonant scattering amplitude, including the magnetic terms, and use these to calculate the magnetic scattering from a surface. Our approach is to model the truncation rods using the standard kinematical approach for chemical truncation rods.[25,29] Magnetic effects are inserted by including the magnetic terms in the scattering amplitudes.[30] The number of photons per second scattered into the detector, n_s, is

$$n_s=(n_i/A_0)\int d\Theta_i d\Theta_s |T(\alpha_i)|^2 |T(\alpha_s)^2 a_i(\Theta_i) a_s(\Theta_s) \frac{d\sigma}{d\Omega}, \tag{1}$$

where n_i is the number of photons per second in the incident beam, A_0 its cross-sectional area, $T(\alpha)$ the Fresnel transmission coefficient which varies with the incident (α_i) and scattered (α_s) angles, and $d\sigma/d\Omega$ is the x-ray scattering cross section. The Fresnel transmission function differs from one only when α_i or α_s are near to the critical angle. The angular distribution of the incident photons is given by $a_i(\Theta_i)$ while the acceptance of the detector is given by $a_s(\Theta_s)$. The magnetic effects on the Fresnel reflectivity recently considered by Matveev and Matveev[31] are beyond the scope of the present data set, and have been neglected.

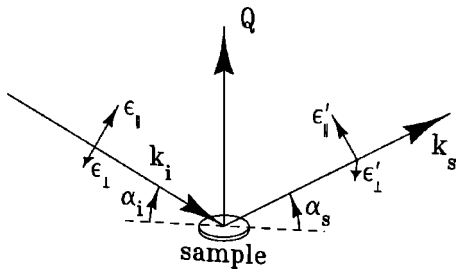

FIG. 3. Scattering diagram showing the linear polarization states of the incident and scattered photons as well as the incident and scattered wave vectors.

The x-ray cross section has been calculated in the kinematical approximation and is given by

$$\frac{d\sigma}{d\Omega}=A\frac{(2\pi r_0)^2}{v^2}\left|\sum_{\text{all atoms } n} f_n(\mathbf{q}) e^{-i\mathbf{q}\cdot\mathbf{r}_n} e^{-W_n(q)}\right|^2, \tag{2}$$

where A is the illuminated surface area, r_0 the Thomson radius, v the unit-cell volume, $\mathbf{r}_n$ the position of the nth atom, and $W_n(\mathbf{q})$ and $f_n(\mathbf{q})$ are the Debye-Waller factor and atomic scattering amplitude, respectively, of atom n. Typically, the outermost planes of atoms are allowed to have Debye-Waller factors which differ from the bulk,[25,29] however, for simplicity, we have used bulk values for the Debye-Waller factors in the fits described below.

The anomalous terms f' and f'' in the atomic form factor $f(\mathbf{q})=f_0(\mathbf{q})+f'+f''$ can become significant when the photon energy is tuned to an absorption edge. Following the work of Hannon *et al.*,[30] these terms may be written within the dipole approximation as

$$f'+f''=\frac{3\lambda}{8\pi}[(F_{11}+F_{1-1})(\boldsymbol{\epsilon}_s^*\cdot\boldsymbol{\epsilon}_i)-i(F_{11}-F_{1-1})(\boldsymbol{\epsilon}_s^*\times\boldsymbol{\epsilon}_i)\times\mathbf{n}+(2F_{10}-F_{11}-F_{1-1})(\boldsymbol{\epsilon}_s^*\cdot\mathbf{n})(\boldsymbol{\epsilon}_i\cdot\mathbf{n})]. \tag{3}$$

Here, the F_{LM} are proportional to the transition probability of order L, where $L=1$ for electric dipole transitions, and contain resonant denominators. It is these resonant terms that produce the enhancements in the magnetic scattering that are observed at absorption edges. The polarization of the incident and scattered photons are $\boldsymbol{\epsilon}_i$ and $\boldsymbol{\epsilon}_s$, respectively, and $\hat{\mathbf{n}}$ is the direction of the magnetic moment of the atom. In our experiments, the incident beam is linearly polarized in the horizontal plane.[10,20] The scattering geometry is illustrated in Fig. 3.

The first term in Eq. (3) has the same polarization dependence as Thomson scattering and is called the anomalous charge scattering amplitude. The second term is responsible for the magnetic scattering observed in our experiments. Due to the $\boldsymbol{\epsilon}_s^*\times\boldsymbol{\epsilon}_i$ factor, the incident σ polarization is rotated into scattered π polarization. The fact that the polarization of the magnetic and charge scattering are orthogonal allows one to utilize a polarization analyzer to distinguish between them.[21] The third term in Eq. (3) produces a resonant second harmonic of the magnetic scattering and is ignored in our analysis. In order to simplify the calculations we treat the

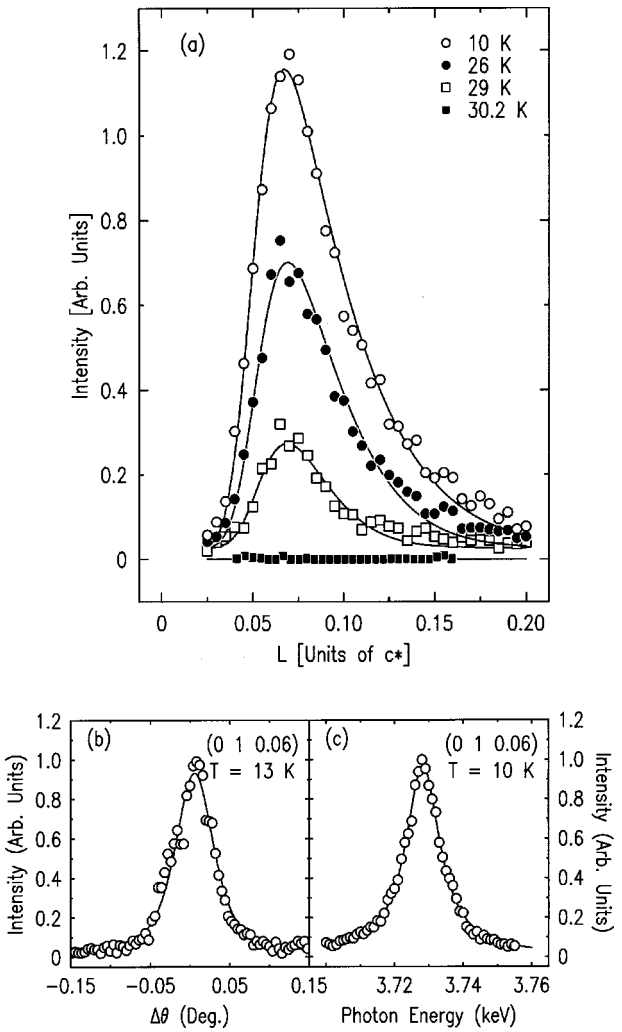

FIG. 4. (a) Intensity along the $(01L)$ magnetic truncation rod at four different temperatures and for an incident photon energy of 3.728 KeV. (b) Rocking curve through the $(01L)$ magnetic truncation rod at $L=0.06c^*$. (c) Scattering intensity of the $(01L)$ magnetic truncation rod as a function of the energy of the incident photon energy.

F_{LM} term in Eq. (3) as a constant, independent of the scattering wave vector q, but fit the energy dependence explicitly. This simplification is reasonable as long as the range of q, considered in the analysis, is limited.

III. RESULTS AND DISCUSSION

A. Nonspecular magnetic truncation rods

The intensity measured along the $(01L)$ magnetic truncation rod [see Fig. 1(b)] is shown in Fig. 4(a) at four different temperatures. This rod corresponds to pure magnetic scattering as seen in Fig. 1(b). Integrated rod profiles, obtained by rocking θ at each L, gave similar results and are not shown. Each nonzero profile increases from $L=0$, takes a maximum at the critical angle, and then falls off for larger L. As the temperature increases, the magnetic scattering weakens, and entirely disppears above $T_N=30.2$ K. The maximum peak intensity at 10 K is of order 10 counts per second at X22C and approximately 200 counts per second at the wiggler beamline X25.

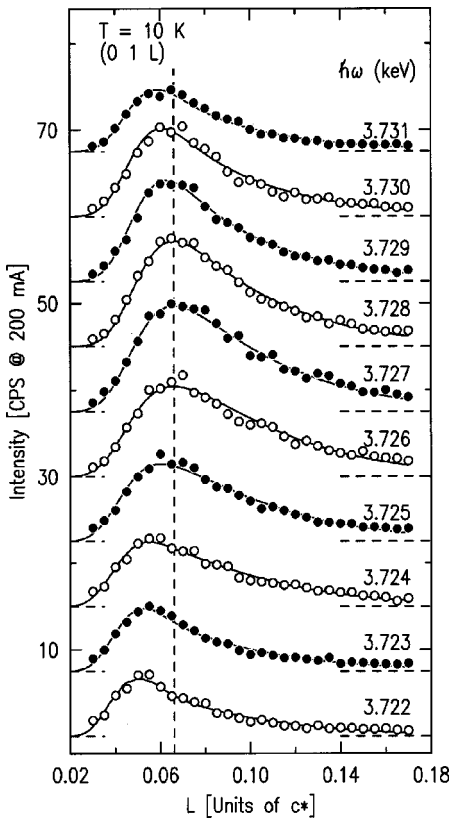

FIG. 5. $(01L)$ magnetic truncation rod profiles for various incident photon energies near to the U M_{IV} edge. Data were obtained at beamline X22C.

Figure 4(b) shows a transverse scan through the $(01L)$ rod at an L of $0.06c^*$. The data are well described by a Lorentzian-squared line shape. The best fit (line) results in a transverse full width at half maximum (FWHM) of 0.06°, which is slightly larger than the bulk mosaic (0.05°). Transverse scans taken at different positions along the rod indicate that the line shape is independent of L although its width increases from 0.05° at small L to approximately 0.15° at $L=0.25c^*$. Both the line shape and FWHM were observed to be independent of temperature at the present signal levels. Quantitative statements about the extent of inplane magnetic order at the surface will require detailed modeling, which is beyond the scope of the present work.

A good test of the origin of the observed scattering is to study its dependence on incident photon energy. If the signal were due to charge rather than magnetic scattering, we might expect that the intensity would still be observable for energies away from the M_{IV} absorption edge. The scattered intensity at (0 1 0.06) is plotted as a function of incident photon energy in Fig. 4(c). The observed resonance is virtually identical to that of the bulk magnetic Bragg reflections[20,32] and is clear evidence that the scattering is magnetic in origin. This is further supported by tests of the scattered polarization, which show that it is predominantly $\sigma\rightarrow\pi$.

The dependence of the magnetic truncation rod profile on the incident photon energy is shown in Fig. 5. At $\hbar\omega=3.722$ keV the peak in the profile appears near $L=0.055$. As the photon energy is increased, it shifts to larger L reaching ≈ 0.068 at the M_{IV} edge. Above the edge, the peak shifts back to lower L as the photon energy is further increased.

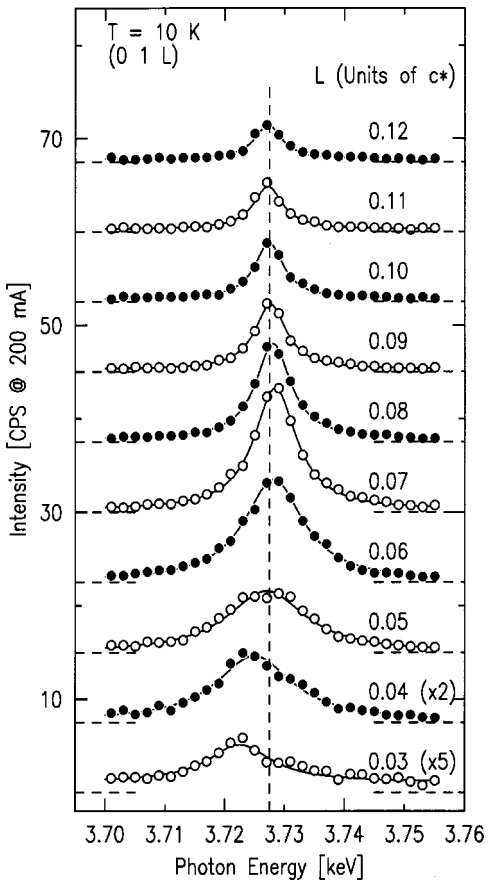

FIG. 6. Intensity of the $(01L)$ magnetic truncation rod as a function of incident photon energy at various positions along the rod. Data were obtained at beamline X22C.

The largest signals occur when the incident and scattered angles α_i and α_s are close to the critical angle for total external reflection. The fact that the peak shifts is not surprising since the critical angle depends on f' and at an absorption edge both the real and imaginary parts of the atomic scattering factor change rapidly with photon energy.[25]

As described in Sec. II D, there are two major contributors to the rod profile: the magnetic structure, which enters through the differential cross section, and the Fresnel transmission coefficients. At angles much larger than the critical angle, the dominant effect is the resonant magnetic scattering amplitude. However, near the critical angle, both the magnetic scattering amplitude and the Fresnel effects are important. This is illustrated in Fig. 6, where the scattered intensity versus incident photon energy is shown at a number of different L. At large values of L, α_i, and α_s are larger than the critical angle, so that a single peak, fixed in position and width, and characteristic of the energy dependence of the magnetic scattering amplitude, is observed. At smaller L, the peak shifts to lower photon energy and broadens. The shift of the peak away from the U M_{IV} edge shows that the Fresnel effects become important at small L.

In order to model the data shown in Figs. 4 and 5 it is necessary to know the atomic scattering factors. Unfortunately, the atomic scattering factors for U are not well known for photon energies near the M edges, and it was necessary to measure them. A variety of techniques for determining the anomalous terms was employed. The collected results are

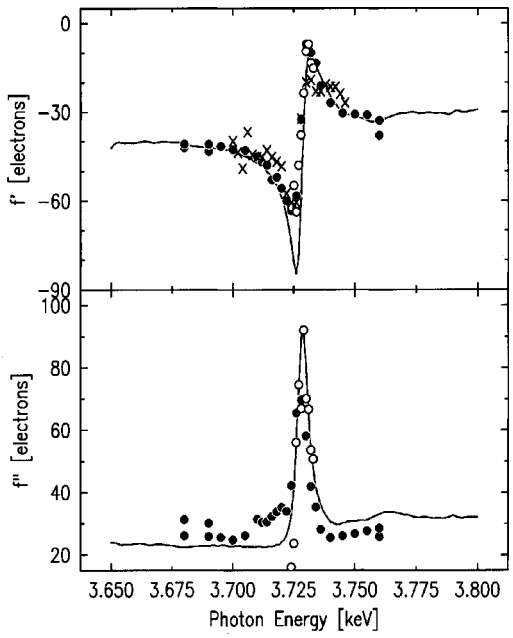

FIG. 7. Anomalous scattering factors for U at the M_{IV} absorption edge. Data are from absorption measurements (solid lines), specular reflectivity near the critical angle (solid circles), shifts in the (220) bulk Bragg reflection (crosses), and from fits to the $(01L)$ magnetic truncation rod profiles (open circles).

compiled in Fig. 7. In one set of experiments, the specular x-ray reflectivity at small angles was utilized to determine f' and f'' (solid circles), following Ref. 33. These measurements suffered from the small size of our samples relative to the large footprint of the beam at grazing incidence, but gave results which agree well with absorption measurements of thin UO_2 films (solid line).[34]

We next fitted the profiles shown in Fig. 4(a) and 5 by assuming that the surface and bulk antiferromagnetic structures are the same at $T=10\,\mathrm{K}$ and then varying the atomic scattering amplitudes with the incident photon energy. The best fits are shown by the solid lines in the figures. The results of these fits (open circles in Fig. 7) are in good agreement with the results from specular reflectivity.

Finally, due to the large change in f' ($\geqslant$50 electrons) at an absorption edge, refraction at the surface is important. As noted many years ago,[35,36] these effects lead to a shift in the position of a bulk Bragg reflection with photon energy, and from this, the real part of the anomalous scattering factor can be determined. The data shown by crosses in Fig. 7 were obtained from measurements of the peak position of the (220) bulk Bragg reflection as a function of photon energy in an earlier experiment.[32]

B. Temperature dependence of nonspecular magnetic truncation rods

In order to characterize the temperature dependence of the near surface magnetic structure, we measured the intensity of the scattering at several positions along the $(01L)$ magnetic truncation rod, including the bulk magnetic reflection at $L=1$. The results obtained for three different L's, are shown in Fig. 8. These data correspond to peak intensities and were obtained by varying the temperature at a fixed scattering

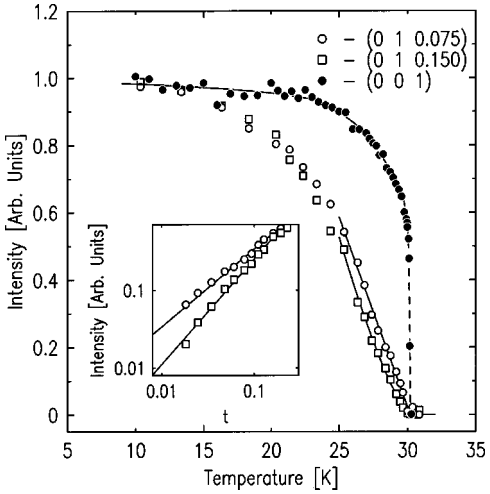

FIG. 8. Temperature dependence of the magnetic scattering at the (001) magnetic bulk Bragg reflection (solid circles) and at various positions along the $(01L)$ magnetic truncation rod (open symbols). Data are normalized to unity at low temperatures. Inset: log-log plot of the scattering intensity at two different positions along the $(01L)$ magnetic truncation rod as a function of reduced temperature. Solid lines are a power-law fit to the data.

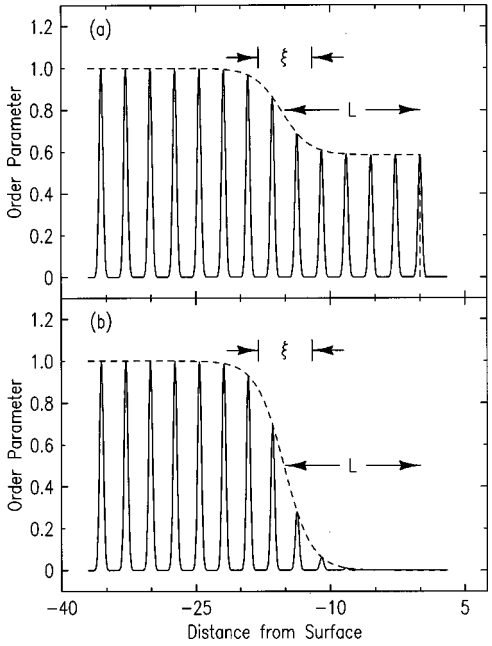

FIG. 9. Models for the absolute value of the magnetization for a few atomic planes near a surface (solid lines) and the associated envelope function (dashed lines). Shown are the thickness of the disordered layer l and the width ξ of the interface separating the ordered bulk from the disordered surface. (a) Surface-induced disorder model of Lipowsky. (b) Model used in our analysis.

wave vector. θ-integrated intensities gave a similar behavior, which is expected from the observed temperature independence of the transverse widths, at least at the present signal levels. Since the atomic planes all scatter in phase at $L=1$, the intensity at the magnetic bulk Bragg reflection is proportional to the square of the magnetic order parameter. Note that, given the strong absorption at the U M_{IV} edge, the penetration depth at the bulk Bragg reflection is less than 1000 Å. Nevertheless, the temperature dependence of the scattering is identical to that observed by neutron scattering.[32] Specifically, the intensity is nearly constant at low temperatures and abruptly drops to zero at T_N, consistent with a discontinuous phase transition.

Interestingly, whereas the temperature dependence of the scattering at the magnetic bulk Bragg reflection appears discontinuous, the scattering along the rod at grazing incidence (open symbols) appears continuous. As illustrated by the insert, which shows the truncation rod results plotted as a function of reduced temperature $[t\equiv(T_N-T)/T_N]$ on a log-log scale, the intensities near T_N are well described by a power law in reduced temperature, $I(t)=I_0t^{2\beta}$. The solid lines give the corresponding fits for temperatures greater than 25 K.

Similar behavior has been observed at the discontinuous chemical order-disorder transformation of Cu_3Au.[17,18,37] In their grazing incidence x-ray scattering studies, Dosch and co-workers[17,18,37] observed that the temperature dependence of the intensity along a truncation rod varied continuously, also following a power-law dependence on reduced temperature. This led them to suggest that the near surface volume is more disordered than the bulk at temperatures near the transition. Further, they found that the temperature dependence of the scattering became more bulklike at larger values of L, which they argued resulted from the increase in penetration depth with L. The collected results were explained in terms of the model of surface-induced disorder introduced by Lipowsky for discontinuous bulk transitions.[14,15]

In Lipowsky's model, the coupling of the disorder at the surface to the underlying order in the bulk leads to an order parameter profile such as shown in Fig. 9(a). Each Gaussian in the figure represents the average sublattice magnetization on the specified atomic plane. The amplitude of the Gaussian reflects the degree of magnetic order with widths that are held fixed. Then, two length scales characterize the falloff of the magnetization at the surface: l, the thickness of the layer at the surface with reduced order, and ξ the width of the interface which separates the magnetically ordered bulk from the disordered surface layer.

Efforts to fit the observed magnetic truncation rods to a magnetic order profile similar to that shown in Fig. 9(a) were unsatisfactory. Specifically, this profile can be considered as having two interfaces, one at the surface of the sample and the other between the ordered bulk and the disordered surface layer. Between the two interfaces the scattering amplitude is reduced. In this regard, the scattering is similar to that of a thin film of a low-density material deposited on a high density substrate, which implies that the truncation rods should have intensity oscillations with a periodicity determined by the thickness of the overlayer. No such oscillations are observed in the magnetic truncation rods of UO_2.

The temperature dependence of the scattering along the $(01L)$ rod in UO_2 also differs from that observed for Cu_3Au in that it apparently becomes more continuous (or *less* bulklike) with increasing L. This can be seen directly in Fig. 8. The exponent which characterizes the temperature dependence of the scattering at $L=0.150$ is larger than that at $L=0.075$ (see inset), leading to a more rounded profile. The fitted values of β obtained from four different runs along $(\phi 1L)$ are plotted as a function of L in Fig. 10. Clearly, β increases with L, in contrast to the results reported for Cu_3Au.[17,18,36]

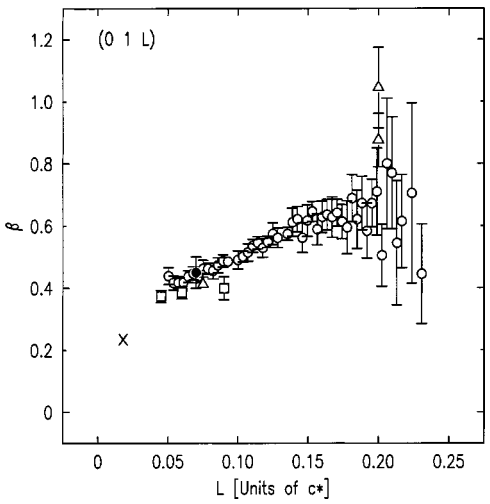

FIG. 10. Variation of the exponent β with position along the $(01L)$ magnetic truncation rod. The results of four separate experiments are shown by the different symbols.

More generally, we have found that β increases not with L, but with ΔL, the separation from bulk Bragg reflections. This is shown in Fig. 11, which shows the value of β deduced along the $(01L)$ rod near the bulk Bragg reflection at $L=1$ and along the specular rod near the bulk Bragg reflection at $L=1$. These data were fitted to a power law in reduced temperature over the same temperature range as in Fig. 10. The fitted values for β are presented as a function of the distance from the nearest bulk Bragg reflection $\|\Delta L\|$. The measured values are in qualitative agreement with each other, and increase with distance from the nearest bulk Bragg reflection.

Since the diffracting planes do not scatter in phase at an arbitrary position along a truncation rod, the scattered intensity at any particular position is not a direct measure of the average magnetic order in the volume determined by the penetration depth. Rather, the intensity at every position along the rod depends on the profile of the magnetic order. For a diffuse (or disordered) interface in which the correlations can be described with a Gaussian function, the scattered intensity $I(\xi,L)$ can be related to the intensity that would be observed for an identical but flat interface I_0 via

$$I(\xi,L)=I_0 e^{(\xi\Delta L)^2}, \tag{4}$$

where ΔL is the distance to the nearest bulk Bragg reflection.[25,29] This is a simple Debye-Waller-like term with the rms roughness replaced by the interfacial width. In the model of surface-induced disorder, the interfacial width varies as a function of the reduced temperature as $\xi(t)=\xi_0\sqrt{\ln(t)}$.[15] Substituting this into Eq. (4) we find that it introduces a temperature dependence to the scattering of the form

$$I(t,L)=I_0 t^{(\xi_0\Delta L)^2}. \tag{5}$$

This implies that the temperature dependence of the scattering along a truncation rod should follow a power-law dependence on reduced temperature with an exponent that increases with ΔL. It is consistent with the general trend of the data of Figs. 10 and 11, however, it complicates the interpretation of the measured exponents in terms of surface induced disorder. In view of the already weak signals, we have not pursued this analysis further.

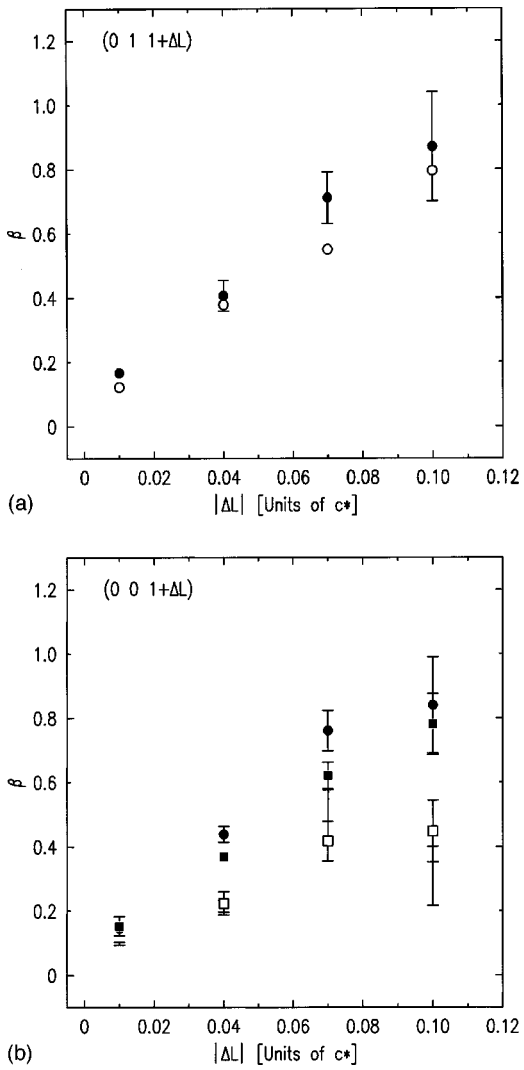

FIG. 11. Variation in the exponent β with position along the rods near the (a) (011) and (b) (001) magnetic bulk Bragg reflections. Solid symbols correspond to $\Delta L>0$ and open symbols to $\Delta L<0$. Lines are a guide to the eye.

C. Specular magnetic reflectivity

The discussion above provided a motivation to refit the truncation rod profiles with the modified Lipowsky profile illustrated in Fig. 9(b), in which the partially disordered magnetic surface layer of thickness l is assumed to be fully disordered. Due to the fact that the penetration depth varies rapidly at small L, it turns out that it is difficult to extract both ξ and l from fitting the truncation rod profiles at higher temperatures. This problem is avoided along the specular rod near the magnetic bulk Bragg reflection at $L=1$ for which α_i and α_s are much greater than the critical angle. As described in Sec. II A, both charge and magnetic scattering contribute to the intensity along the specular direction for temperatures below T_N. However, the charge scattering may be considerably reduced by using polarization analysis and accepting only the $\sigma\rightarrow\pi$ rotated signal.

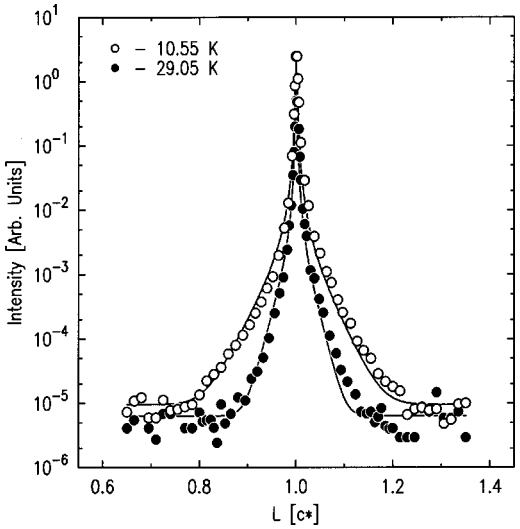

FIG. 12. Magnetic specular reflectivity (circles) obtained near the (001) reflection using a polarization analyzer to suppress the charge scattering background.

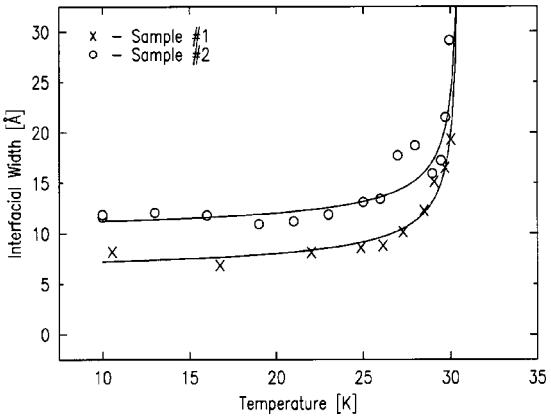

FIG. 13. Temperature dependence of the derived magnetic interfacial widths for two different samples.

The specular magnetic reflectivity obtained in the neighborhood of the bulk (001) reflection is presented in Fig. 12 for two temperatures. The intensity of the magnetic scattering at the bulk reflection is over 300 000/sec and falls off by five orders of magnitude within a few tenths of an inverse Å. The wings of the scattering are clearly much weaker at higher temperatures near $T_N = 30.2$ K (open circles) than at 10 K (closed circles). This suggests that the magnetic interface is more diffuse at higher temperatures, since broadly speaking a sharper profile in reciprocal space is consistent with a more extended density profile in real space.

Fits of the specular and truncation rod intensities were made to a model of the magnetic interface, consisting of an interfacial width ξ and thickness l of magnetically disordered volume (see Fig. 9). The magnetic profiles were otherwise assumed to match the profile of the electronic charge density, which was also determined using reflectivity techniques. The latter correspond closely to ideal termination, supplemented by a thin absorbing layer. The best fits are shown by the solid lines in Figs. 4(a) and 12. The thickness of the disordered layer l was found to be relatively insensitive to variations in the temperature, and could be fixed at a value of about 13 Å. The corresponding value of the interfacial width at low temperatures (10 K) was about 6 Å. Thus, in contrast to the electronic charge density, the magnetic structure is disordered very near the surface, and has a more rounded profile, even at 10 K in the magnetically ordered phase.

For increasing temperatures, the interfacial width exhibited a dramatic increase, starting at about 25 K and diverging as T approached T_N. This is illustrated in Fig. 13 where the fitted widths are plotted versus temperature for two different UO_2 (001) samples (samples 1 and 2). Whereas the limiting values of the disordered volume and interfacial width of the two samples are different at low temperatures (6 vs 11 Å), the temperature dependencies appear similar. The divergence of the widths near T_N is qualitatively consistent with the theory of surface induced disorder, which predicts a logarithmic increase. The limited range of L over which the magnetic reflectivity has been obtained limit us to qualitative conclusions in the present study. Even smoother and cleaner samples will be required in experiments carried out at third generation sources before more quantitative conclusions can be drawn. We are nevertheless encouraged that both the encapsulated and oxidized samples (1 and 2) give such similar results for the temperature dependence of the interfacial width. It suggests that the effects we are observing are intrinsic, or at least, not strongly dependent on the thin oxide surface layer.

IV. SUMMARY AND CONCLUSIONS

Resonant x-ray magnetic scattering was used to determine the magnetic structure near the (001) surface of the antiferromagnetic oxide UO_2 by direct measurement of the magnetic reflectivity and truncation rods. For temperatures near to, but below, the bulk Néel temperature, there is a magnetically disordered layer at the surface approximately 8 Å in thickness (in sample 1). A magnetic interface, separating the magnetically disordered surface layer from the magnetically ordered bulk exists at all temperatures below the Néel temperature. At the lowest temperatures studied this magnetic interface has a width of slightly more than one lattice constant. With increasing temperature, the interfacial width increases and appears to diverge at the Néel temperature. This leads to a continuous variation of the surface magnetic scattering near the magnetic ordering transition, in contrast to the bulk which is discontinuous. The magnetic scattering along the rods further exhibits a power-law behavior in reduced temperature, with an exponent that increases with increasing separation from bulk Bragg peaks.

These results are qualitatively consistent with the theory of surface induced disorder, and motivate continued effort on smoother and still-cleaner samples at third generation synchrotron sources. In particular, our specular reflectivity studies of the chemical surface at 8-keV photon energy indicate that approximately 10 Å of a superoxide may exist at the surface on both samples 1 and 2. It is still possible that the near-surface behavior observed in these samples is in part due to the effect of excess oxygen on the magnetic structure, which is known to decrease T_N.[38] Whether the excess oxygen acts only to disorder the near surface region at zero temperature and the resulting temperature dependence of the

magnetization profile is governed by a Lipowsky-type model, or whether the magnetic order profile is determined at all temperatures by the doping profile, is unknown. Further experiments on carefully prepared samples with stoichiometric surfaces are underway to test these ideas. The preliminary results obtained for the encapsulated sample in the present study are very encouraging.

ACKNOWLEDGMENTS

We would like to thank V. Meyritz for help with the sample preparation. Work at Brookhaven was supported by the U.S. DOE under Contract No. DE-AC02-98CH10886. B.D.G. acknowledges financial support from NSERC of Canada, OCMR of Ontario.

[1] G. A. Prinz, Nature (London) **250**, 1092 (1990).
[2] W. L. O'Brien and B. P. Tonner, Phys. Rev. B **52**, 15 332 (1995).
[3] See, for example, J. G. Tobin, K. W. Goodman, F. O. Schumann, R. F. Willis, J. B. Kortright, J. D. Denlinger, E. Rotenberg, A. Warwick, and N. V. Smith, Surf. Sci. **395**, L227 (1998).
[4] A notable exception to this is neutron reflectometry. See, for example, G. P. Felcher, R. T. Kampwirth, K. E. Grey, and R. Felici, Phys. Rev. Lett. **52**, 1539 (1984).
[5] A. Fasolino, P. Carra, and M. Altarelli, Phys. Rev. B **47**, 3877 (1993); G. P. M. Poppe and A. Fasolino, Surf. Sci. **331**, 1186 (1995).
[6] C.-C. Kao, J. B. Hastings, E. D. Johnson, D. P. Siddons, G. C. Smith, and G. A. Prinz, Phys. Rev. Lett. **65**, 373 (1990).
[7] J. F. MacKay, C. Teichert, D. E. Savage, and M. G. Lagally, Phys. Rev. Lett. **77**, 3925 (1996).
[8] J. M. Tonnerre, L. Sève, D. Raoux, G. Soullié, B. Rodmacq, and P. Wolfers, Phys. Rev. Lett. **75**, 740 (1995).
[9] C.-C. Kao, C. T. Chen, E. D. Johnson, J. B. Hastings, H.-J. Lin, G. H. Ho, G. Meigs, J.-M. Brot, S. L. Hulbert, Y. U. Idzerda, and C. Vettier, Phys. Rev. B **50**, 9599 (1994); M. Sacchi, J. Vogel, and S. Iacobucci, J. Magn. Magn. Mater. **147**, L11 (1995); V. Chakarian, Y. U. Idzerda, C.-C. Kao, and C. T. Chen, *ibid.* **165**, 52 (1997); J. W. Freeland, V. Chakarian, Y. U. Idzerda, S. Doherty, J. G. Zhu, J.-H. Park, and C.-C. Kao, Appl. Phys. Lett. **71**, 276 (1997); M. Sacchi, C. F. Hague, E. M. Gullikson, and J. H. Underwood, Phys. Rev. B **57**, 108 (1998).
[10] D. B. McWhan, C. Vettier, E. D. Isaacs, G. E. Ice, D. P. Siddons, J. B. Hastings, C. Peters, and O. Vogt, Phys. Rev. B **42**, 6007 (1990).
[11] S. Ferrer, J. Alvarez, E. Lindgren, X. Torrelles, P. Fajardo, and F. Boscherini, Phys. Rev. B **56**, 9848 (1997).
[12] S. F. Alvarado, M. Campagna, and H. Hopster, Phys. Rev. Lett. **48**, 51 (1982).
[13] D. Weller, S. F. Alvarado, W. Gudat, K. Schroden, and M. Campagna, Phys. Rev. Lett. **54**, 1555 (1985).
[14] R. Lipowsky, Phys. Rev. Lett. **49**, 1575 (1982); R. Lipowsky and W. Speth, Phys. Rev. B **28**, 3983 (1983).
[15] R. Lipowsky, Ferroelectrics **73**, 69 (1987).
[16] W. Schweika, D. P. Landau, and K. Binder, Phys. Rev. B **53**, 8937 (1996).
[17] H. Dosch, L. Mailander, H. Reichart, J. Peisl, and R. L. Johnson, Phys. Rev. B **43**, 13 172 (1991).
[18] H. Reichert, P. J. Eng, H. Dosch, and I. K. Robinson, Phys. Rev. Lett. **74**, 2006 (1995).
[19] G. M. Watson, D. Gibbs, G. H. Lander, B. D. Gaulin, L. E. Berman, Hj. Matzke, and W. Ellis, Physica B **221**, 405 (1996); Phys. Rev. Lett. **77**, 751 (1996).
[20] C. C. Tang, W. G. Stirling, G. H. Lander, D. Gibbs, W. Herzog, P. Carra, B. T. Thole, K. Mattenberger, and O. Vogt, Phys. Rev. B **46**, 5287 (1992).
[21] D. Gibbs, G. Grübel, D. R. Harshman, E. D. Isaacs, D. B. McWhan, D. Mills, and C. Vettier, Phys. Rev. B **43**, 5663 (1991).
[22] B. C. Frazer, G. Shirane, D. E. Cox, and C. E. Olsen, Phys. Rev. **140**, A1448 (1965); B. T. M. Willis and R. I. Taylor, Phys. Rev. Lett. **17**, 188 (1965).
[23] O. G. Brandt and C. T. Walker, Phys. Rev. **170**, 528 (1968).
[24] J. Faber and G. H. Lander, Phys. Rev. B **14**, 1151 (1976).
[25] R. Feidenhans'l, Surf. Sci. Rep. **10**, 105 (1989); I. K. Robinson and D. J. Tweet, Rep. Prog. Phys. **55**, 599 (1992).
[26] G. C. Allen, P. M. Tucker, and J. W. Tyler, Vacuum **32**, 481 (1982).
[27] T. N. Taylor and W. P. Ellis, Surf. Sci. **77**, 321 (1978); **107**, 249 (1981).
[28] Hj. Matzke and A. Turos, J. Nucl. Mater. **114**, 349 (1983); Solid State Ionics **49**, 189 (1991); A. Turos, R. Falcone, A. Drigo, A. Sambo, L. Nowicki, N. Madi, J. Jagielski, and Hj. Matzke, Nucl. Instrum. Methods Phys. Res. B **118**, 659 (1996).
[29] D. Gibbs, B. M. Ocko, D. M. Zehner, and S. G. J. Mochrie, Phys. Rev. B **42**, 7330 (1990).
[30] J. P. Hannon, G. T. Trammell, M. Blume, and D. Gibbs, Phys. Rev. Lett. **61**, 1245 (1988).
[31] V. M. Matveev and V. V. Matveev, Physica B **208-209**, 768 (1995).
[32] G. M. Watson, B. D. Gaulin, D. Gibbs, T. R. Thurston, P. J. Simpson, S. M. Shapiro, G. H. Lander, Hj. Matzke, S. Wang, and M. Dudley, Phys. Rev. B **53**, 686 (1996).
[33] F. Stanglmeier, B. Lengeler, W. Weber, H. Gobel, and M. Schuster, Acta Crystallogr., Sect. A: Found. Crystallogr. **A48**, 626 (1992).
[34] J. O. Cross, M. Newville, J. J. Rehr, L. B. Sorenson, C. E. Bouldin, G. M. Watson, T. Gouder, G. H. Lander, and M. I. Bell, Phys. Rev. B **58**, 11 215 (1998).
[35] R. W. James, *The Optical Principles of the Diffraction of X Rays* (G. Bell and Sons, London, 1962).
[36] J. M. Cowley, Phys. Rev. **77**, 669 (1950); J. Appl. Phys. **21**, 24 (1950).
[37] H. Dosch, L. Mailander, A. Lied, J. Peisl, F. Grey, R. L. Johnson, and S. Krummacher, Phys. Rev. Lett. **60**, 2382 (1988); H. Dosch and J. Peisl, Colloq. Phys. **50**, C7-257 (1989).
[38] A. Arrott and J. E. Goldman, Phys. Rev. **108**, 948 (1957).